Kovove Mater. 63 2025 263–270
DOI: 10.31577/km.2025.5-6.263

An investigation into the microstructure of coating defects produced in a zinc melt with aluminum additives

Olga Sergeevna Bondareva[1], Hamid M. Mahan[2], Sherwan Mohammed Najm[3]*, Tomasz Trzepieciński[4]

[1] *Samara National Research University, 443086 Samara, Russia*
[2] *Baqubah Technical Institute, Middle Technical University, 10074 Baghdad, Iraq*
[3] *Department of Fuel and Energy Engineering Techniques, College of Oil & Gas Techniques Engineering – Kirkuk, Northern Technical University, 36001 Kirkuk, Iraq*
[4] *Department of Manufacturing Processes and Production Engineering, Rzeszów University of Technology, 35-959 Rzeszów, Poland*

Received 11 May 2025, received in revised form 22 November 2025, accepted 24 November 2025

Abstract

This study aims to investigate the structure and chemical composition of zinc-aluminum coatings with a grain defect. Defects and irregularities, such as localized thickening and adhered "grains," were noticed in the coating obtained from the Zn + 7 wt.% Al melts at 480 °C. As a solution, it was observed that the galvanizing temperature range of 410–460 °C maintains a thickness of 8–13 μm. At 480 °C, the coating thickness increases to 35–40 microns, and local defects in the form of grains measuring 110–120 microns appear. By analyzing the binary systems Al-Fe, Fe-Zn, and Zn-Al, and the ternary system Zn-Al-Fe, conclusions were drawn about the phase composition of the defect and the possible reasons for its occurrence. Finally, the steps to rectify this issue have been outlined.

K e y w o r d s: hot-dip galvanizing, Zn-Fe-Al system, Zn-Al coating, microstructure, intermetallic dross, coating defect

1. Introduction

Hot-dip galvanizing (HDG) is the process of coating steel with molten zinc. In recent decades, HDG has been inextricably linked to the alloying of molten zinc with various additives to enhance the coating's corrosion resistance and regulate its thickness and structure [1]. The most common alloying elements are lead, bismuth, and tin. These metals enhance the fluidity of liquid zinc, positively affecting zinc consumption and improving the appearance of coatings. However, despite their beneficial effects, their presence in the bath is controversial due to the increased risk of liquid metal cracking [2]. Zinc melts are often alloyed with aluminum, magnesium, and nickel [3, 4]. Researchers are also investigating the introduction of new experimental additives, such as titanium, manganese, copper, cerium, and boron, into the galvanizing process [5–9]. The complex influence of three ingredients at once is interesting [10–15].

A comprehensive economic analysis of zinc mining indicates that total global zinc resources are approximately 250 million tons. Due to the high demand for this metal and ever-increasing consumption, especially in anti-corrosion protection, global reserves can only cover demand for the next 17 years [16]. As a result, the issue of reducing the thickness of the zinc coating while maintaining, and even increasing, its corrosion resistance is becoming increasingly urgent. Aluminum is one of the most commonly used elements for alloying with zinc in the molten state. Aluminum microadditives at concentrations up to 0.005 wt.% are used to enhance the brightness of the coating. Additionally, additives containing up to 0.06 wt.% aluminum have been used to control increases in coating thickness during the galvanization process [17]. Fe-Al intermetallic compounds are formed at the interface between molten Zn and the Fe base with a 0.1–0.2 wt.% concentration of Al. They act as a diffusion barrier, regulating reactions between Fe and molten Zn and in-

*Corresponding author: e-mail address: sherwan@ntu.edu.iq

Table 1. Chemical composition (in wt.%) of S235JR steel according to EN 10025-2 standard

C	Si	Mn	P	S	N	Cu	Fe
< 0.17	–	< 1.40	< 0.035	< 0.035	< 0.012	< 0.55	Bal.

Table 2. Mechanical properties of S235JR steel

Yield strength (MPa)	Ultimate tensile strength (MPa)	Hardness HB
235	360–510	104–154

fluencing subsequent reactions between Fe and molten Zn [18].

Galfan, a zinc-based alloy containing 5 wt.% aluminum and 0.05 wt.% mischmetal, entered the industry in the 1980s. A smooth surface, low thickness, high corrosion resistance, and ductility characterize coatings of this alloy on steel. It has been established that Galfan has a multilayer structure consisting of thin, alternating layers with a high concentration of zinc and aluminum, and intermediate layers of very thin thickness. Thanks to this microstructure, Galfan has unique plasticity and corrosion resistance [19, 20]. Researchers have observed that zinc bath containing 1–20 wt.% Al generates a layer with structural isomorphism to $FeAl_3$ on the iron surface. Others have found that this layer, which stops the reaction, is an intermetallic Fe_2Al_5 that contains zinc. As the Al content in the zinc bath increases, the hot-dip coating reaction layer becomes thicker [21].

Many researchers note that the presence of Al increases the corrosion resistance of coatings [22]. This is due to the structural characteristics of ZnAl coatings, which consist of a FeAl intermetallic phase diffusion layer and an outer layer. FeAl intermetallic compounds have excellent corrosion resistance [23]. Increased resistance to corrosion is ensured by the appearance of corrosion products on the surface of the coating: ZnO, $ZnAl_2O_4$, and Al_2O_3, as well as the subsequent formation of hydrocarbonates $Zn_6Al_2(OH)_{16}CO_3 \cdot 4H_2O$, $Zn_2Al(OH)_6Cl \cdot 2H_2O$, and/or $Zn_5Cl_2(OH)_8 \cdot H_2O$ [23–25]. Researchers have also demonstrated the high corrosion resistance of zinc-aluminum coatings by combining UV irradiation with an alternating cycle of wetting and drying in a NaCl solution, and at various ambient temperatures [26, 27].

However, alloying zinc melt with aluminum can lead to several technological difficulties. One problem in the electroplating industry is the formation of iron-based intermetallic compounds (IMCs) in the Al-Zn plating bath due to the dissolution of iron from steel products. These kinds of IMCs primarily cause scale formation in the Al-Zn bath [29]. This causes point metal defects in coated steel products, and dross builds up in the Al-Zn bath. Another problem is the appearance of drops of different densities in zinc-aluminum baths, some of which can sink to the bottom, while others can float in the melt. So, intermetallic particles were found in ZnAl baths on continuous galvanizing lines. Their make-up changed depending on how much aluminum was in the bath: ζ-$FeZn_{13}$ at low concentrations; at δ-$FeZn_{10}AI_Y$ intermediate concentrations; and η-$Fe_2Al_5Zn_X$ at higher concentrations. These intermetallic compounds comprise a significant portion of the industry-recognized waste known as "dross." Due to the density of the intermetallic phases relative to liquid Zn, ζ-$FeZn_{13}$, and δ-$FeZn_{10}AI_Y$ are referred to as "bottom dross," while η-$Fe_2Al_5Zn_X$ is called "top dross" [30].

This study examined coatings made in a Zn + 7 wt.% Al melt and found "grain" defects. These could be local thickenings or dross particles that have stuck together in the melt. Such a coating defect spoils the appearance of the coating, depriving it of smoothness and shine. The goal was to investigate the structure and elemental composition of zinc-aluminum coatings with a "grain" defect to determine the cause and identify possible solutions.

2. Materials and methods

For the experiments, samples measuring 50 mm × 50 mm × 3 mm were prepared from sheet steel grade S235JR, as specified in EN 10025-2, with three samples per galvanizing temperature. All measurement results are the average of at least 5 similar measurements per sample. The chemical composition of steel is given in Table 1. The mechanical properties are shown in Table 2.

Table 3 displays the chemical composition of the samples as determined by the Foundry-Master XPR optical emission spectrometer. The process steps for preparing the samples comprised cleaning, degreasing, pickling, fluxing, and drying. Then they were immersed in molten zinc containing 7 wt.% aluminum. The galvanizing temperature was 410–480 ℃, and the immersion time in the melted zinc was 2 minutes. Af-

T a b l e 3. Measured chemical composition of S235JR steel (in wt.%)

Fe	C	Si	Mn	P
99.30	0.14	0.02	0.35	0.03

Fig. 1. HV-1000 microhardness tester.

ter cooling, the coating thickness was measured with a magnetic thickness gauge.

The surface preparation was conducted using a Remet LS2 grinding and polishing machine, yielding fully prepared samples. The chemical composition and microstructure of the coatings were analyzed using a TESCAN VEGA SB scanning electron microscope equipped with an OXFORD INCA X-act energy dispersive spectrometer. As shown in Fig. 1, an HV1000 microhardness tester was used with a load of 50 g. Five measurements of each coating phase were taken to determine the microhardness of the steel and the structural components of the coating in the defect area. Before hot-dip galvanizing, the steel substrate had a microhardness of 123 HV.

3. Results

Research has shown that in the galvanizing temperature range of 410–460 ℃, the coating thickness is constant and amounts to 8–13 microns (Fig. 2). At a temperature of 480 ℃, the average thickness of the coating increases to 35–40 microns, and local defects in the form of grains with a thickness of 110–120 microns appear on the coating. A coating with such defects has a rough surface and poor appearance. Figure 3 displays the appearance of coating samples with and without defects.

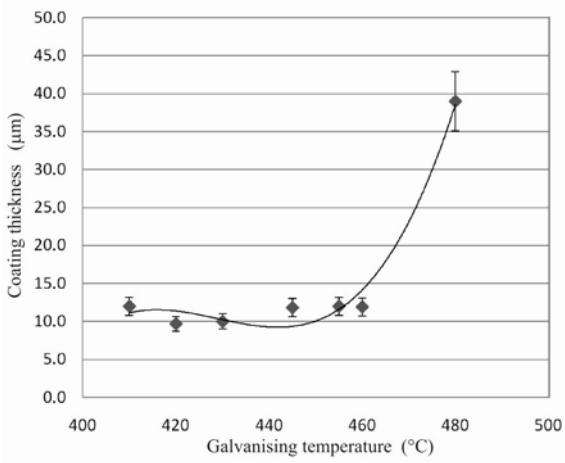

Fig. 2. Effect of galvanizing temperature on coating thickness.

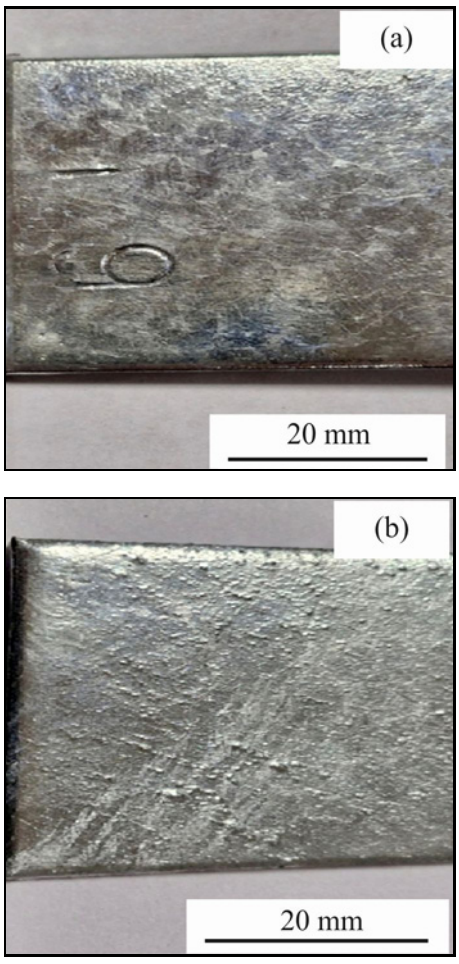

Fig. 3. Coated samples: (a) defect-free and (b) with surface defect.

A melt temperature of 410–460 ℃ throughout the examination process resulted in a defectless (Fig. 3a), high-quality coating with a thickness of 8–13 microns.

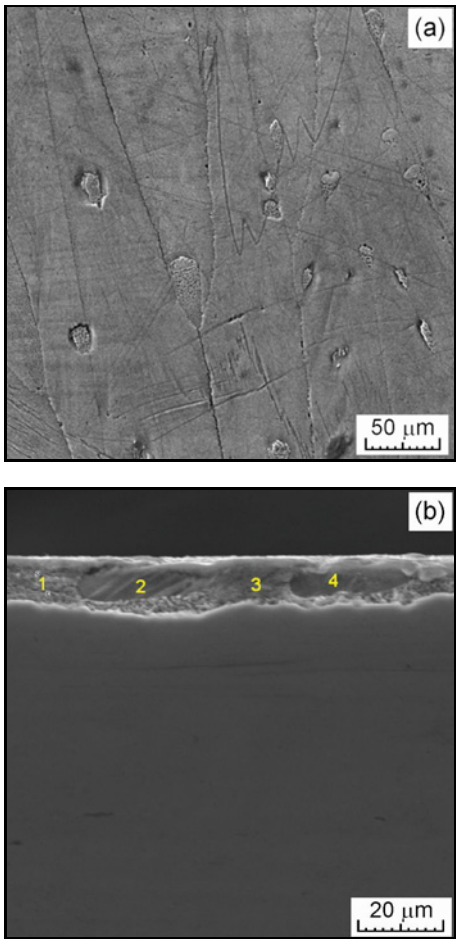

Fig. 4. SEM micrographs of (a) surface morphology of the coating and (b) microstructure in the sample cross-section with points 1–4 used for chemical analysis.

Under other conditions, surface defects were observed (Fig. 3b). Figure 4 displays SEM micrographs of the coating's surface and microstructure.

The coating exhibits visible precipitates of the excess phase surrounded by a finely dispersed mixture of phases. The excess phase (points 2 and 4 in Fig. 4b) contains 3.8–5.6 wt.% aluminum, 3.5 wt.% iron, and the rest is zinc. The finely dispersed mixture (points 1 and 3 in Fig. 4b) contains approximately 28–29 wt.% aluminum and 2.5–3.5 wt.% iron; the remainder is zinc.

A "granular pimples" defect forms on the coating at a melt temperature of 480 ℃. The SEM micrographs of the coating surface and microstructure of the coating with a defect are shown in Figs. 5a and 5b, respectively.

Additionally, another finding was that the cross-section of the coating defect shows areas of varying structure. A chemical analysis of the structural components was conducted to determine the phase composition at points 1–4, as marked in Fig. 5b. Table 4 presents the results of the chemical analysis at these points.

The results of chemical analysis showed that in the coating defect in the form of a "grain", there are structural areas containing 53–56 wt.% aluminum, 33–38 wt.% iron, and 9–12 wt.% zinc (points 1 and 3 in Fig. 5b), alternating with layers of defect-free coating (points 2 and 4 in Fig. 5b).

The qualitative elemental distributions, as determined by EDS mapping, are shown in Fig. 6. The mapping reveals that the intermetallic compound formed at the steel substrate/coating interface etches back to the original sample surface.

Finally, Fig. 7 shows that the microhardness of the excess phase and fine-grained mixture of phases is about 120 HV50, and the microhardness of the intermetallic inclusions is about 204 HV50.

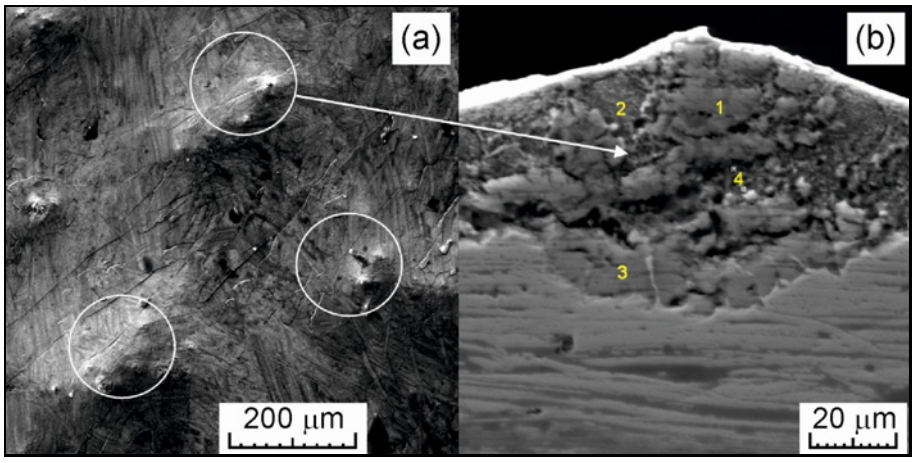

Fig. 5. SEM micrographs of coating with a "grain" defect: (a) surface and (b) microstructure with points used for chemical analysis.

Table 4. Chemical analysis of the structural components of the coating defect (in wt.%)

Chemical analysis points	Al	Fe	Zn	Sum
1	55.70	32.58	11.73	100.00
2	1.45	1.22	97.34	100.00
3	53.28	38.03	8.69	100.00
4	5.22	3.42	91.36	100.00

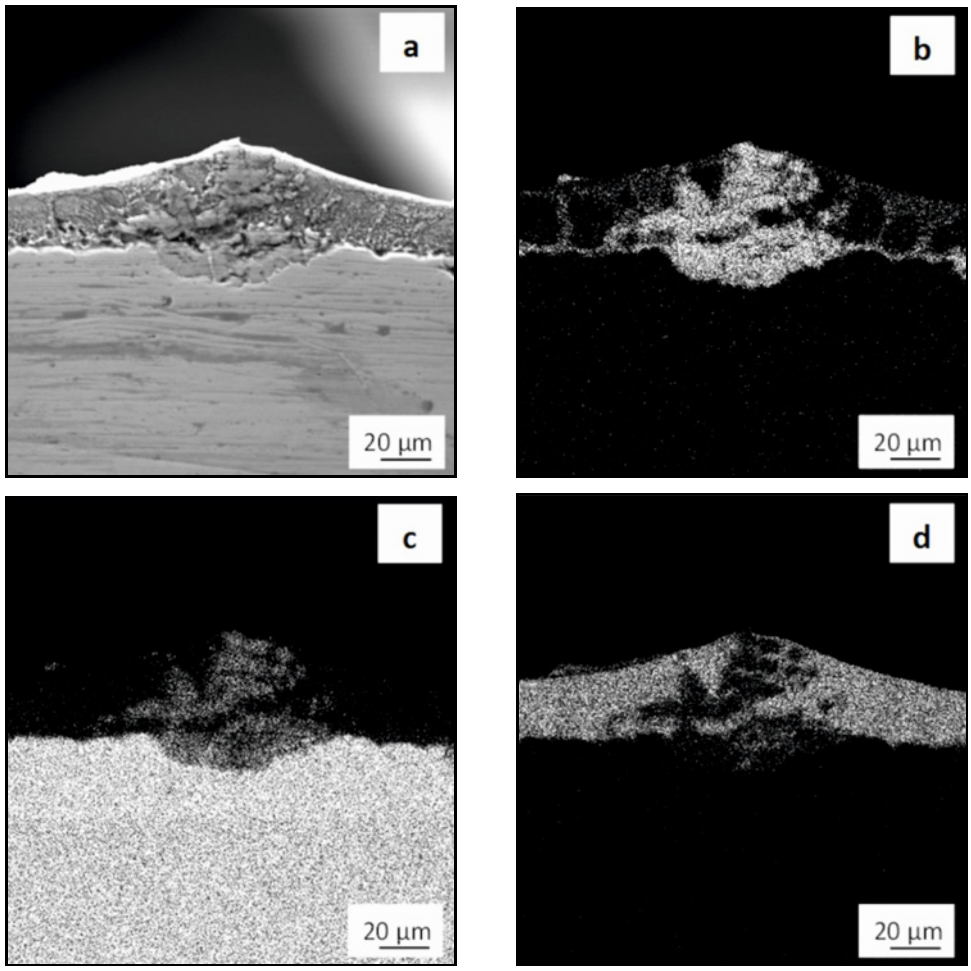

Fig. 6. EDS mapping of elements over the cross-sectional area of the coating defect: a) SEM micrograph and elemental distribution (Kα1) of (b) Al, (c) Fe, and (d) Zn.

4. Discussion

The analysis of the coating microstructure results must be based on data from binary and ternary diagrams and on the coating's main components, namely Al-Fe-Zn. Figure 8 displays the binary systems of interacting metals.

It is known that during hot galvanizing of steel in pure zinc at a temperature of 430–480 ℃, a coating is formed consisting of intermetallic phases by the Fe-Zn system: Γ, Γ_1, δ, and ζ (Fig. 8a). However, in the presence of aluminum additives in the zinc melt, according to the Al-Fe phase diagram at a galvanizing temperature of 410–480 ℃, three intermetallic phases can form in the coating: $FeAl_2$, Fe_2Al_5, and $FeAl_3$ (Fig. 8b). These phases inhibit the formation of Fe-Zn intermetallic compounds.

The molten zinc with 7 wt.% aluminum, upon cooling and forming a coating on the steel, crystallizes to form primary grains of the excess phase containing about 5 wt.% aluminum, 3.5 wt.% iron, and 92 wt.% zinc. The excess phase is surrounded by a continuous layer of fine-grained eutectic phase mixture, the chemical composition of which is 28 wt.% aluminum, 3 wt.% iron, and 67 wt.% zinc, which corresponds to a eutectoid mixture of α and β solid solutions (Fig. 8c).

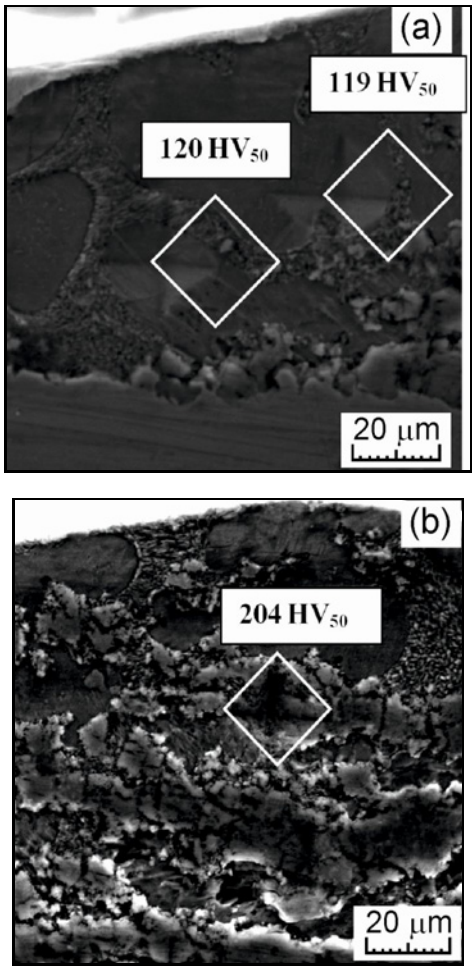

Fig. 7. Microhardness of the structural components (a) in the defect-free area and (b) in the defect area.

Defects in the form of intermetallic inclusions in the coating obtained by increasing the melt temperature to 480 °C have a chemical composition of 53–56 wt.% aluminum, 33–38 wt.% iron, and 9–12 wt.% zinc. To identify these inclusions, it is necessary to analyse the Zn-Al-Fe ternary diagram, which has been studied in detail in [30, 32–35].

The three-part system was studied in [31], and it was found that the intermetallic compounds in the bad coating consist of the α'-FeAl+, $FeAl_2$+, and Fe_2Al_5 phases. In the Fe-Al binary system [31], the highest amount of Zn that can dissolve is 1.9 at.% in the ζ-$FeAl_2$ phase and 14.9 at.% in the η-Fe_2Al_5 phase. McDermid et al. [36] found that η-$Fe_2Al_5Zn_X$ contains 9.85 ± 1.2 at.% Zn or 16.67 ± 1.8 wt.% Zn. By comparing the chemical composition of defective inclusions with that of known intermetallic compounds, it was found that the defects are most likely due to the η-$Fe_2Al_5Zn_X$ phase. The EDS mapping results showed that the IMCs in the coating defect do not adhere to the melt dross. A "grains" defect is formed due to the

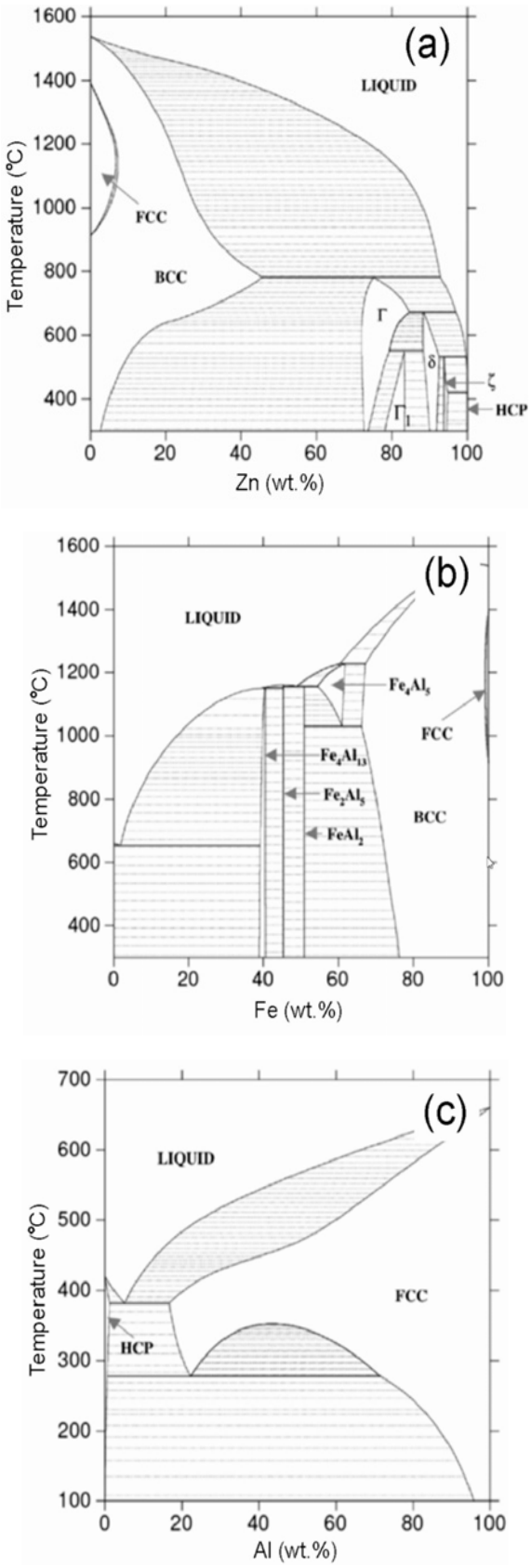

Fig. 8. Phase diagrams of binary systems: (a) Fe-Zn, (b) Al-Fe, and (c) Zn-Al [34].

diffusion interaction of iron from the base with the zinc-aluminum melt.

It can be assumed that with an increase in the galvanizing temperature to 480 °C, the rate of diffusion of iron from the substrate increases, which leads to an increase in the thickness of the Fe_2Al_5 intermetallic compound on the surface, its enrichment in zinc, and the formation of local thickenings in the form of "grains" on the surface. To eliminate this defect, it is recommended not to exceed the melt temperature of 460 °C.

5. Conclusions

As a result of the work carried out, the change in the thickness of the Zn-7 wt.% Al coating with increasing melt temperature in the range of 410–480 °C was shown, and the microstructure and chemical composition of the coating deposited on steel substrate at temperatures of 440 and 480 °C were studied. In the coating microstructure obtained at 440 °C, primary grains of the excess phase were observed, containing about 5 wt.% aluminum, 3.5 wt.% iron and 92 wt.% zinc. The excess phase is surrounded by a continuous layer of a fine-grained mixture of phases, the chemical composition of which is 28 wt.% aluminum, 3 wt.% iron, and 67 wt.% zinc, which corresponds to a eutectoid mixture of α and β solid solutions. At a temperature of 480 °C, defects in the coating in the form of local thickenings – "grains" were observed. It was established that the thickenings are an intermetallic compound η-$Fe_2Al_5Zn_X$. The microhardness of the excess phase and fine-grained mixture of phases is 120 HV50, and the microhardness of the intermetallic inclusions is about 204 HV50. Finally, the recommendation is not to exceed the melt temperature above 460 °C to eliminate the "grain" defect.

References

[1] O. S. Bondareva, O. S. Dobychina, Overview of zinc melt alloying systems for hot dip galvanizing, Chernye Met. 12 (2022) 76–85. (in Russian) https://doi.org/10.17580/chm.2022.12.11

[2] K. Henryk, S. Mariola, Benefits and limitations of the use of Pb, Sn, and Bi alloying elements in hot dip galvanizing bath: A review, J. Mater. Eng. Perform. 32 (2023) 5680–5688. https://doi.org/10.1007/s11665-023-08005-1

[3] Q. Liu, Y. Cao, S. Chen, X. Xu, M. Yao, J. Fang, K. Lei, G. Liu, Hot-dip galvanizing process and the influence of metallic elements on composite coatings, J. Compos. Sci. 8 (2024) 160. https://doi.org/10.3390/jcs8050160

[4] Z. W. Chen, N. F. Kennon, J. B. See, M. A. Barter, Technigalva and other developments in batch hot-dip galvanizing, JOM 44 (1992) 22–26. https://doi.org/10.1007/BF03222746

[5] K. Bracka-Kęsek, A. Szczęsny, E. Guzik, D. Kopyciński, Evaluation of effect of Ti addition to zinc bath on kinetics of growth of alloy layer formed in process of hot-dip galvanisation on steel substrate, Materials 16 (2023) 4773. https://doi.org/10.3390/ma16134773

[6] S. Grandhi, V. S. Raja, S. Parida, Effect of manganese addition on the appearance, morphology, and corrosion resistance of hot-dip galvanized zinc coating, Surf. Coat. Technol. 421 (2021) 127377. https://doi.org/10.1016/j.surfcoat.2021.127377

[7] C. Bellini, V. D. Cocco, F. Iacoviello, L. P. Mocanu, Bath chemical composition influence on intermetallic phases damage in hot dip galvanizing, Procedia Struct. Integr. 39 (2022) 574–581. https://doi.org/10.1016/j.prostr.2022.03.131

[8] W. Chen, Y. Liu, H. Tu, C. Wu, X. Su, J. Wang, The effects of B on the microstructure and corrosion resistance of Zn-6Al-3Mg alloy coating, Steel Res. Int. 95 (2024) 2400180. https://doi.org/10.1002/srin.202400180

[9] G. Wang, H. Lu, P. Li, X. Li, Y. Wang, Effect of cerium on the microstructure and anti-corrosion performance of Al-Zn coatings, Surf. Coat. Technol. 473 (2023) 130046. https://doi.org/10.1016/j.surfcoat.2023.130046

[10] J. Zhao, C. Ding, G. Wu, J. Zhang, Role of aluminium on liquid metal embrittlement susceptibility for Zn–Al–Mg/Sn coated hot-formed steels, J. Mater. Res. Technol. 19 (2022) 747–764. https://doi.org/10.1016/j.jmrt.2022.05.092

[11] A. Chakraborty, R. Ghosh, M. Sudan, A. Mondal, Improvement in hot dip galvanized coating microstructure and properties by pre-metallic deposition on steel surface: A comprehensive review, Surf. Coat. Technol. 449 (2022) 128972. https://doi.org/10.1016/j.surfcoat.2022.128972

[12] J. W. Lee, I. Son, S. J. Kim, Newly designed surface control using Si addition in trace quantity for Zn-2Al-3Mg alloy coated steel sheet with improved corrosion resistance, Appl. Surf. Sci. 598 (2022) 153868. https://doi.org/10.1016/j.apsusc.2022.153868

[13] T. Guo, Y. Wang, L. Yu, Y. Jin, B. Zeng, B. Dou, X. Liu, X. Lin, Roles of Al and Mg on the microstructure and corrosion resistance of Zn-Al-Mg hot-dipped coated steel, Materials 17 (2024) 1512. https://doi.org/10.3390/ma17071512

[14] J. S. Park, J. W. Lee, S. J. Kim, Corrosion mechanism according to localized damage of Zn-Al-Mg alloy coated steel sheet used in plant farm, Corros. Sci. Technol. 22 (2023) 123–130. https://doi.org/10.14773/CST.2023.22.2.123

[15] Z. Ma, C. Ding, R. Lu, Z. Chen, G. Wu, J. Zhang, Effect of Al and Sn on the microstructure, microhardness and corrosion properties of Zn-Al-Mg coatings, Mater. Today Commun. 33 (2022) 104892. https://doi.org/10.1016/j.mtcomm.2022.104892

[16] H. Kania, M. Saternus, Evaluation and current state of primary and secondary zinc production—A review, Appl. Sci. 13 (2023) 2003. https://doi.org/10.3390/app13032003

[17] T. Min, Y. Gao, X. Huang, Z. Gong, K. Li, S. Ma, Effects of aluminium concentration on the formation of inhibition layer during hot-dip galvanizing, Int. J. Heat Mass Transf. 127 (2018) 394–402. https://doi.org/10.1016/j.ijheatmasstransfer.2018.08.016
[18] H. Kania, L. Komorowski, The influence of the chemical composition of a zinc bath upon corrosion resistance of coatings obtained on sebisty steel, Solid State Phenom. 246 (2016) 85–90. https://doi.org/10.4028/www.scientific.net/SSP.246.85
[19] H. Kania, Corrosion and anticorrosion of alloys/metals: The important global issue, Coatings 13 (2023) 216. https://doi.org/10.3390/coatings13020216
[20] A. Mesbahzadeh, H. Abdolmaleki, Z. S. Seyedraoufi, A. Mesbahzadeh, A. Ahmadi, K. Mirzavand, Y. Shajari, H. Bakhtiari, Interfacial investigation of St13/Molten Zn–5%Al and corrosion behavior of formed layer via hot-dip process, Surf. Eng. Appl. Electrochem. 57 (2021) 124–135. https://doi.org/10.3103/S1068375521010087
[21] X. Zhu, Y. Shen, Y. Ge, S. Zhang, Effect of hot dip plating process parameters on microstructure and properties of zinc–10% aluminum–mischmetal alloy coated for bridge cable steel wire, Metals 12 (2022) 1257. https://doi.org/10.3390/met12081257
[22] T. Kato, K. Nunome, K. Kaneko, H. Saka, Formation of the ζ phase at an interface between an Fe substrate and a molten 0.2 mass% Al-Zn during galvannealing, Acta Mater. 48 (2000) 2257–2262. https://doi.org/10.1016/S1359-6454(00)00037-9
[23] S. Shawki, Z. A. Hamid, Effect of aluminium content on the coating structure and dross formation in the hot-dip galvanizing process, Surf. Interface Anal. 35 (2003) 943–947. https://doi.org/10.1002/sia.1608
[24] H. C. Shih, J. W. Hsu, C. N Sun, S. C. Chung, The lifetime assessment of hot-dip 5% Al-Zn coatings in chloride environments, Surf. Coat. Technol. 150 (2002) 70–75. https://doi.org/10.1016/S0257-8972(01)01508-0
[25] X. Zhang, C. Leygraf, I. O. Wallinder, Atmospheric corrosion of Galfan coatings on steel in chloride-rich environments, Corros. Sci. 73 (2013) 62–71. https://doi.org/10.1016/j.corsci.2013.03.025
[26] A. Fornalczyk, J. Cebulski, P. Dorota, The morphology of corrosion products in FeAl alloys after heat-resistance tests at different temperatures, Solid State Phenom. 227 (2015) 409–412. https://doi.org/10.4028/www.scientific.net/SSP.227.409
[27] J. Pan, Y. Wang, L. Yang, W. Li, D. Yang, B. Dou, C. Hu, X. Li, Effect of UV irradiation on the alternating wet and dry corrosion behavior of galvanized steel in sodium chloride solution, Crystals 13 (2023) 1195. https://doi.org/10.3390/cryst13081195
[28] Y. Liang, B. He, G. Fu, S. Wu, B. Fan, Effects of ambient temperature and state of galvanized layer on corrosion of galvanized steel in high-humidity neutral atmosphere, Materials 16 (2023) 3656. https://doi.org/10.3390/ma16103656
[29] A. Khaliq, V. Kasva, A. S. Alghamdi, M. Ramadan, T. Subhani, W. Haider, K. S. A. Halim, Iron intermetallic compounds (IMCs) formation mechanism in the molten aluminium zinc (Al-Zn) coating alloy, Teh. Vjesn. – Tech. Gaz. 31 (2024) 460–465. https://doi.org/10.17559/TV-20230523000660
[30] V. Raghavan, Al-Fe-Zn (Aluminium-Iron-Zinc), J. Phase Equilibria Diffus. 29 (2008) 431–433. https://doi.org/10.1361/105497103772084606
[31] I. Lee, K. Han, I. Ohnuma, R. Kainuma, Experimental determination of phase diagram at 450 °C in the Zn-Fe-Al ternary system, J. Alloys Compd. 854 (2021) 157163. https://doi.org/10.1016/j.jallcom.2020.157163
[32] A. R. Marder, F. E. Goodwin, Chapter 3 – Zn coating phase equilibria, in: A. R. Marder, F. E. Goodwin (Eds.), The metallurgy of zinc coated steels, Elsevier, Amsterdam 2023, pp. 35-48. https://doi.org/10.1016/B978-0-323-99984-7.00019-1
[33] N. Y. Tang, X. Su, On the ternary phase in the zinc-rich corner of the Zn-Fe-Al system at temperatures below 450 °C, Metall. Mater. Trans. A. 33 (2002) 1559–1561. https://doi.org/10.1007/s11661-002-0078-5
[34] J. Nakano, D. V. Malakhov, S. Yamaguchi, G. R. Purdy, A full thermodynamic optimization of the Zn-Fe-Al system within the 420–500 °C temperature range, Calphad 31 (2007) 125–140. https://doi.org/10.1016/j.calphad.2006.09.003
[35] G. Ghosh, M. Palm, Al-Fe-Zn ternary phase diagram evaluation, MSI Eureka 96 (2023) 10.17658.4.5.
[36] J. R. McDermid, M. H. Kaye, W. T. Thompson, Fe solubility in the Zn-rich corner of the Zn-Al-Fe system for use in continuous galvanizing and galvannealing, Metall. Mater. Trans. B 38 (2007) 215–230. https://doi.org/10.1007/s11663-007-9028-3